Chemical Science

ROYAL SOCIETY OF CHEMISTRY

REVIEW

View Article Online
View Journal | View Issue

Cite this: *Chem. Sci.*, 2021, **12**, 9885

Enzyme-activatable fluorescent probes for β-galactosidase: from design to biological applications

Yongkang Yao, Yutao Zhang, Chenxu Yan, Wei-Hong Zhu and Zhiqian Guo *

β-Galactosidase (β-gal), a typical hydrolytic enzyme, is a vital biomarker for cell senescence and primary ovarian cancers. Developing precise and rapid methods to monitor β-gal activity is crucial for early cancer diagnoses and biological research. Over the past decade, activatable optical probes have become a powerful tool for real-time tracking and *in vivo* visualization with high sensitivity and specificity. In this review, we summarize the latest advances in the design of β-gal-activatable probes *via* spectral characteristics and responsiveness regulation for biological applications, and particularly focus on the molecular design strategy from turn-on mode to ratiometric mode, from aggregation-caused quenching (ACQ) probes to aggregation-induced emission (AIE)-active probes, from near-infrared-I (NIR-I) imaging to NIR-II imaging, and from one-mode to dual-mode of chemo-fluoro-luminescence sensing β-gal activity.

Received 13th April 2021
Accepted 27th June 2021

DOI: 10.1039/d1sc02069b

rsc.li/chemical-science

1. Introduction

β-Galactosidase (β-gal), as a typical glycoside hydrolase enzyme, can catalyse the hydrolysis of the β-glycosidic bond and convert the lactose into monosaccharide. It is a widely held view that β-gal is closely associated with primary ovarian cancers and cell senescence.[1–3] For instance, metastatic ovarian cancer cells (*e.g.* SKOV3 and OVCAR3) exhibit a higher level of β-gal activity relative to normal human cells.[4] Moreover, β-gal is commonly used as a reporter enzyme to study gene expression and regulation in biological systems, especially for *Escherichia coli* β-galactosidase, which is well characterized and encoded by the *LacZ* gene.[5–7] Various methods have been developed to evaluate β-gal activity for biological research, including colorimetry,[8,9] electrochemistry,[10,11] positron emission tomography (PET),[12] magnetic resonance imaging (MRI)[13–15] and so forth. For instance, chromogenic probe X-gal (5-bromo-4-chloro-3-indolyl-β-D-galactopyranoside) is known for β-gal expression staining in histology, but due to its poor cell-permeability, it needs to fix cells or sacrifice organisms, making it difficult to perform *in vivo* imaging.[8,16,17]

Fluorescence techniques provide a powerful way to visualize dynamic biological processes in living cells and organisms owing to their high detection sensitivity, excellent resolution and non-invasive real-time detection abilities.[18,19] In particular, fluorescence imaging in the near-infrared window (NIR-I, 650–900 nm; NIR-II, 1000–1700 nm) has gained more attention and been designed for biological analytes/microenvironmental factors.[20–24] Comparison with the emission falling into the visible region, these NIR fluorophores could effectively decrease background interference and achieve deeper penetration with superior imaging qualities.[25–27] In general, fluorescent probes are divided into two main categories of "always-on" probes and activatable probes. Indeed, activatable probes could switch the fluorescence from the "off" to the "on" state (turn-on probes) or adjust the dual-emission ratio (ratiometric probes) upon activation by a specific target, thus achieving a lower limit of detection and higher signal-to-noise ratio.[28] Considering that current β-gal detection is generally based on β-gal-catalyzed enzyme reaction, elaborately activatable NIR fluorescent probes are expected to realize sensitive and real-time detection, thereby assessing the biological activity of β-gal with high specificity.

The primary themes for activatable probe design and application are the use of spectral characteristics of fluorophores and the strategy employed to regulate its responsiveness. The key properties of fluorophore scaffolds include finely tuning spectroscopic properties and brightness, regulating the wavelength to the NIR region, and uniting multiple modalities for β-gal imaging. Here, we focus on the latest progress in the design of enzyme-activatable fluorescent probes, especially for monitoring β-gal activity in live cells and *in vivo* application. We highlight the rational design strategy for constructing versatile platforms of activatable β-gal probes (Fig. 1), including from turn-on mode to ratiometric mode with accurate quantification, from aggregation-caused quenching (ACQ) to aggregation-

Key Laboratory for Advanced Materials, Institute of Fine Chemicals, Feringa Nobel Prize Scientist Joint Research Center, Frontiers Science Center for Materiobiology and Dynamic Chemistry, School of Chemistry and Molecular Engineering, East China University of Science and Technology, Shanghai 200237, China. E-mail: guozq@ecust.edu.cn

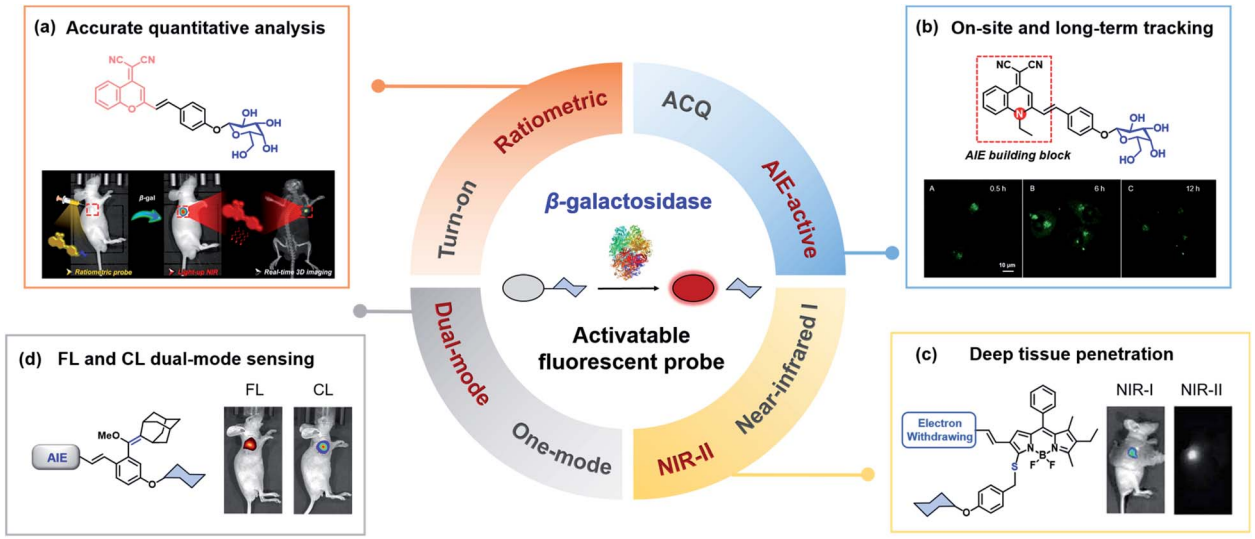

Fig. 1 Design of enzyme-activatable fluorescent probes for *in vivo* sensing β-galactosidase: (a) from turn-on mode to ratiometric mode with accurate quantitative analysis, (b) from the aggregation-caused quenching (ACQ) probe to the aggregation-induced emission (AIE)-active probe with on-site and long-term tracking, (c) from NIR-I to NIR-II wavelength with deeper penetration, and (d) dual-modality of fluorescence and enriched chemiluminescence (CL) imaging with high sensitivity detection.

induced emission (AIE)-active probes with long-term tracking properties, from the NIR-I to the NIR-II wavelength region with deeper penetration, and dual-modality of fluorescence and enriched chemiluminescence (CL) imaging with high sensitivity. In addition, we also constrain our survey to the β-gal-catalyzed reaction by removing the trigger moiety and liberating the activated moiety for magnetic resonance imaging (MRI) and photoacoustic imaging β-gal.

2. Turn-on NIR fluorescent probes for β-gal

Current fluorescent probes display "always-on" signals regardless of interactions with targets, which results in a low signal-to-background ratio and restricts the detection limit. In contrast, turn-on fluorescent probes can be specifically activated by biological targets with remarkable emission from a dark background, thus improving the sensitivity and resolution of bioimaging.[29–31] Generally, turn-on probes for β-gal are built by covalently introducing a β-D-galactopyranoside group as the β-gal-triggered moiety into fluorophores, which could quench the initial emission (off-state). Upon reaction with β-gal, the locked fluorophores would be released and display bright fluorescence emission (on-state). According to this design strategy, Nagano *et al.* reported a wide range of turn-on probes, comprising conventional fluorescein dyes and its analogues for detecting β-gal, but most of their emission falls into the visible range.[4,7,32,33]

In order to enhance the *in vivo* performance, much effort has been made to develop suitable NIR fluorophores as the signal moiety.[34–39] As is well known, commercially available ICG dye – an FDA approved NIR contrast agent with good biocompatibility and biodegradability – is widely employed as a fluorescent reporter. Shabat and co-workers developed a turn-on NIR probe (QCy7-βgal) for the imaging of β-gal (Fig. 2), which contains a NIR cyanine fluorophore (QCy7) and an enzyme-activatable group (β-D-galactopyranoside).[34] The only probe QCy7-βgal displayed almost no fluorescence in the NIR region. Upon incubation with β-gal, QCy7-βgal underwent a cleavage reaction with the broken β-glycosidic bond and subsequently released the active Cy7 fluorophore through self-immolation. Turn-on NIR emission at 720 nm was observed owing to the distinctive change in their π-conjugated system, along with an obvious color change from original yellow to dark (Fig. 2b and c). Based on the advantages of high selectivity and NIR fluorescence, the probe was successfully applied in living mice. As shown in Fig. 2d, the *in vivo* experiments indicated that QCy7-βgal exhibited a significant NIR fluorescence enhancement toward β-gal, showing good biocompatibility and a high signal-to-background ratio.

Considering that de-acidification is a unique characteristic of lysosomes in senescent cells, it is important to distinguish

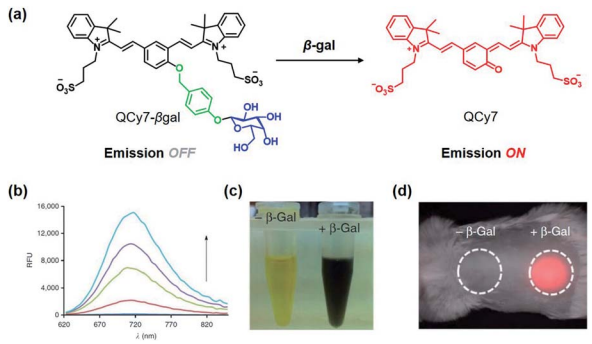

Fig. 2 (a) Fluorescence response of the NIR fluorescent probe QCy7-βgal to β-gal. Fluorescence response (b), absorbance response (c), and *in vivo* imaging (d) of QCy7-βgal.

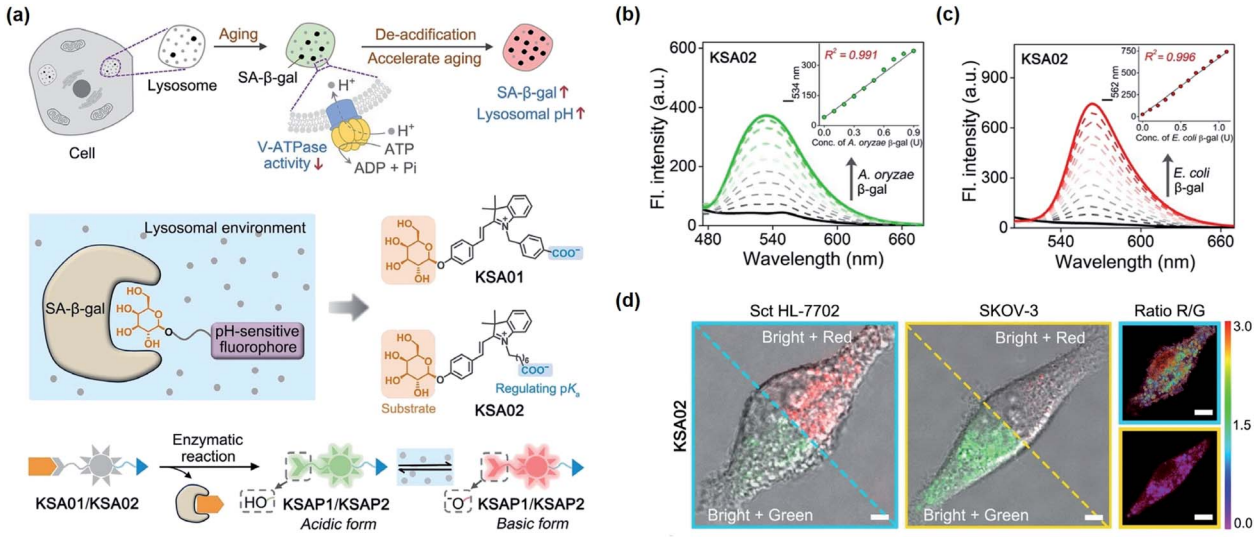

Fig. 3 (a) Two-dimensional SA-β-gal fluorescent probes. (b) Fluorescence response at a short wavelength (534 nm), and (c) at a long wavelength (562 nm), (d) cell imaging of SA-β-gal and cancer-associated β-gal.

senescence-associated β-galactosidase (SA-β-gal) from other endogenous β-gal. Very recently, Guo and co-workers presented two-dimensional fluorescent probes (KSA01 and KSA02) to specifically track cellular senescence (Fig. 3a).[40] These probes were designed by endowing merocyanine-based fluorescent dyes with carboxyl groups, so that they could monitor senescence in a second dimension: lysosomal pH. Upon the addition of *A. oryzae* β-gal (pH 4.0), the galactose moiety of KSA02 was removed to liberate the phenolic hydroxyl moiety, showing green fluorescence at a short wavelength (534 nm) (Fig. 3b). Differently, upon adding *E. coli* β-gal (pH 7.4), KSA02 liberated the phenolic oxygen anion and emitted at a long wavelength (562 nm) (Fig. 3c). Furthermore, based on the fact that senescent cells exhibit higher lysosomal pH than ovarian cancer cells, the probes were successfully evaluated in senescent HL-7702 cells and ovarian cancer-associated SKOV-3 cells. As depicted in Fig. 3d, KSA02 mainly produced a red fluorescence in HL-7702 cells but a green fluorescence in SKOV-3 cells, indicating sensitive differentiation of SA-β-gal from cancer-associated β-gal.

3. Ratiometric probes for quantitative analysis

The library of activatable fluorescent probes with light-up and/or ratiometric modes could dramatically enlarge the quantitative determination. The light-up mode of probes could possess high sensitivity owing to enhanced fluorescent signals from a dark background.[31] However, considering only a single emission channel, these turn-on probes inevitably suffer from analyte-independent interference, such as instrumental parameters and light-scattering by the detection environment.[41] In contrast, ratiometric probes could achieve self-calibration by calculating the signal ratio of two or more independent channels, thereby providing accurate quantitative analysis.[28,41,42] To date, several design strategies have been explored for ratiometric sensing of β-gal activities, including intramolecular charge transfer (ICT),[16,42,43] Förster resonance energy transfer (FRET),[44,45] excited-state intramolecular proton transfer (ESIPT),[46] *etc.*

Recently, Guo *et al.* constructed two ratiometric NIR probes (DCM-βgal and BODIPY-βgal) for β-gal (Fig. 4a), which depends on optimizing the incorporated electron-withdrawing unit to regulate the ICT process.[47,48] Specifically, dicyanomethylene-4*H*-pyran (DCM) and the 4,4-difluoro-4-bora-3*a*,4*a*-diaza-*s*-indacene (BODIPY) fluorophore are utilized as NIR signal reporters, and the D-galactose unit is functionalized as a β-gal triggered moiety. When reacting with β-gal, the D-galactose unit of DCM-βgal and BODIPY-βgal could be specifically hydrolyzed to form phenol, a strong electron-donating group (EDG), thus providing a remarkable ICT-based switch for ratiometric NIR analysis. For DCM-βgal, its initial absorption peak at 440 nm declined, and the new peak extended to 535 nm, accompanied by an obvious yellow-to-rose color change (Fig. 4b). The fluorescence signals remarkably decreased at 500 nm and concurrently increased at 685 nm, thereby obtaining a good linear relationship between the intensity ratio ($I_{685\ nm}/I_{500\ nm}$) and β-gal concentration ($R^2 = 0.98845$) (Fig. 4c). In light of its ratiometric NIR mode, endogenous β-gal in OVCAR-3 cells was quantitatively detected and imaged by the probe DCM-βgal (Fig. 4d and e). More importantly, DCM-βgal allows for high resolution three-dimensional mapping of β-gal activity in living mice (Fig. 4f and g). Considering that DCM has been a commercial dye since 1989,[49] DCM-βgal could be easily synthesized and employed as a potential optical tool for ratiometric measurement of β-gal under physiological conditions. And this work was also highlighted by *Nature Methods* due to its excellent abilities for real-time tracking β-gal *in vivo*.[50]

4. AIE-active probes for on-site sensing and long-term tracking

Fluorescent probes capable of long-term tracking of special enzymes or other biomarkers are in high demand for early

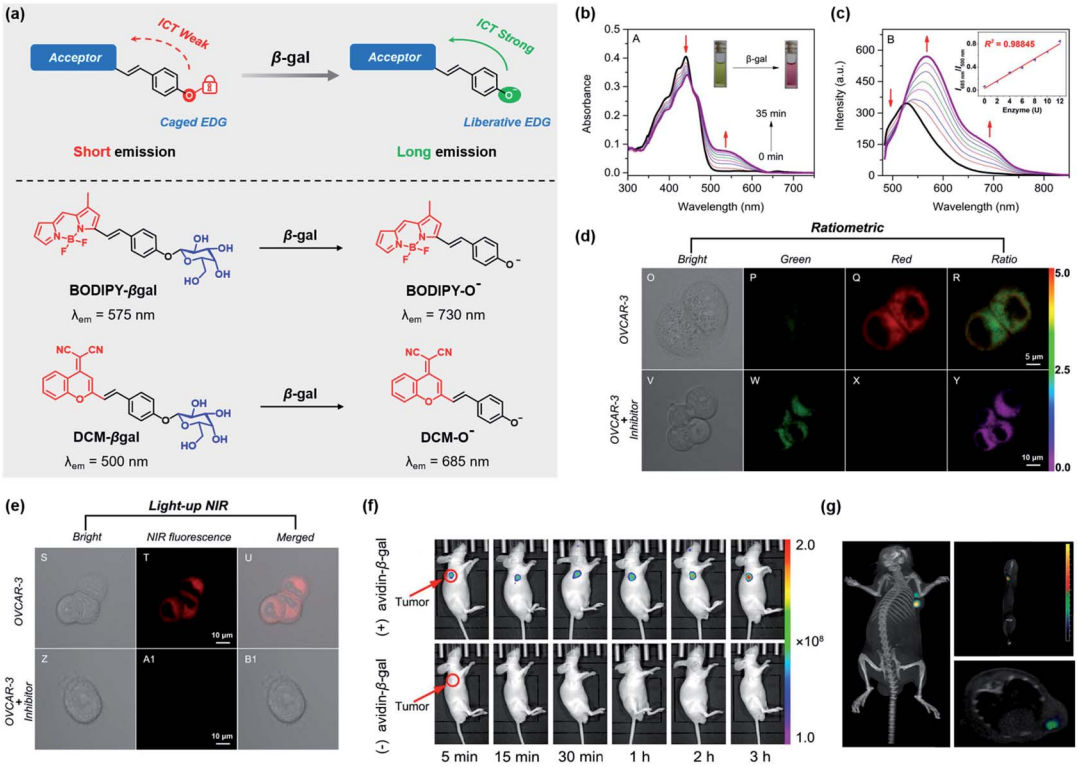

Fig. 4 Ratiometric probes for quantitative analysis: (a) proposed sensing mechanism of DCM-βgal and BODIPY-βgal based on the ICT-induced process. Absorption (b) and emission spectra (c) of DCM-βgal with the presence of β-gal. Images of ratiometric (d) and light-up NIR fluorescence (e) of OVCAR-3 cells with or without the inhibitor of β-gal. (f) *In vivo* images of living mice treated with or without avidin-β-gal. (g) Three-dimensional mapping of β-gal in the mouse model.

detection of diseases.[51–54] Even though current small-molecule fluorescent probes have advantages of quick diffusion and deep penetration into living cells, these probes and/or their enzyme-catalyzed products suffer from easily diffusing across the cell membrane and/or being extruded out. Thus, it is difficult to precisely obtain *in situ* information of these small-molecule activatable probes, owing to their limitation of on-site accumulation and retention time.[19,32,55] Particularly, the aggregation-caused quenching (ACQ) effect is another hardship for these available fluorescent probes at high concentration, leading to distorted *in situ* signals.

As a pioneering study, Tang and co-workers discovered a fascinating photophysical phenomenon, aggregation-induced emission (AIE).[56–58] Different from typical ACQ fluorophores (*e.g.*

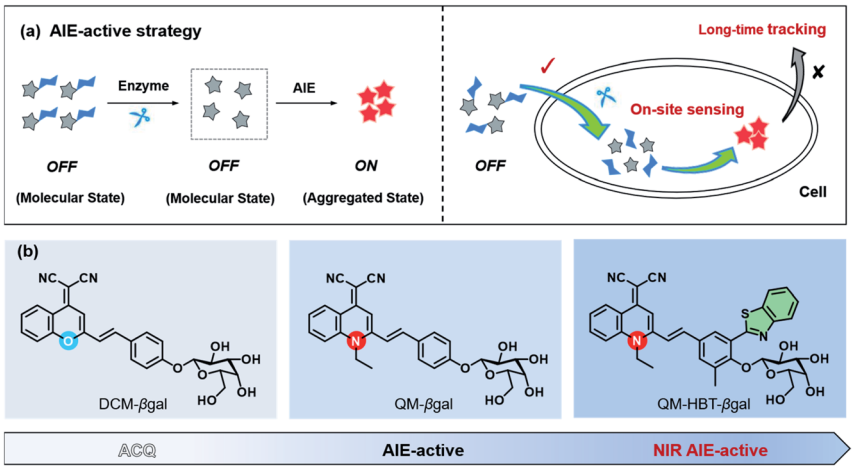

Fig. 5 AIE-active probes for on-site sensing and long-term tracking. (a) AIE-active strategy: introducing a hydrophilic responsive unit into the AIE fluorophore, then efficient enzyme-catalyzed reaction resulting in *on-site* generation of AIE nanoaggregates with an enhanced retention effect. (b) Rational design from the ACQ probe to the AIE-active NIR probe.

fluorescein[59] and rhodamine[60]), AIE luminogens (AIEgens) generally displayed weak or no fluorescence in their molecular state but strong fluorescence in their aggregated state. Notably, the more AIEgens aggregate, the brighter their emission becomes, making them become a kind of promising material for tracking biomolecules with high fidelity in living systems. Recently, some typical AIE fluorescent probes based on the tetraphenylethene (TPE) core have been reported for the detection of β-gal.[61,62] For example, Ding and co-workers developed a β-gal-responsive AIE probe that could selectively identify and remove senescent cancer cells through enzyme-activatable self-assembly and efficient reactive oxygen species (ROS).[62]

However, the initial state of AIE-active probes before the probes interacting with targets of interest is generally "always-on", thereby leading to a "*false-positive*" signal. In this regard, it is necessary to develop an AIE-active strategy to form *in situ* AIE nanoaggregates, enhancing retention for long-term imaging and performing turn-on fluorescence (Fig. 5a). Specifically, the AIE probes with a hydrophilic moiety display good solubility in the physiological environment; when reacting with enzymes, a highly efficient enzyme-catalyzed hydrolysis reaction could liberate hydrophobic AIEgens, followed by *in situ* aggregation to form nanoparticles with intensive emission at the activation site, and the nanoaggregates promote diffusion-resistant on-site sensing in living cells.

Recently, Guo *et al.* elaborately designed a new AIE building block of quinoline-malononitrile (QM), which just incorporates the *N*-ethyl group to replace the oxygen atom of the DCM core. Subsequently, an AIE-active probe (QM-βgal) was developed for tracking β-gal (Fig. 5b and 6a).[63] Because of the hydrophilic β-gal-activatable unit bestowing favorable water-solubility, QM-βgal almost showed very weak emission in aqueous solution; while activated by β-gal, the hydrophobic QM-OH was *in situ* generated and converted into nanoaggregates, accompanied by remarkable fluorescent enhancement at 560 nm (Fig. 6b). Meanwhile, the plot of fluorescence intensity $I_{560\ nm}$ against the concentration of β-gal shows a good relationship ($R^2 = 0.992$) (inset of Fig. 6b). To verify that this AIE-active strategy could achieve on-site sensing and long-term imaging, the typical ACQ probe DCM-gal was chosen as a control for the *in vivo* imaging experiment. As shown in Fig. 6c and d, the incubation time in SKOV-3 ovarian cancer cells prolonged over 12 h, but the intracellular fluorescent signals from QM-βgal were still observed and accumulated with low background interference in living cells.

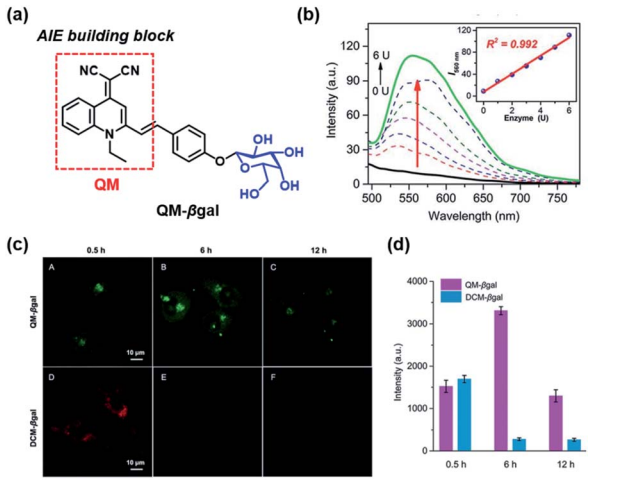

Fig. 6 (a) Chemical structure of QM-βgal. Fluorescence response (b), long-term cell images (c) and averaged fluorescence intensity (d) of QM-βgal.

Furthermore, to extend the emission wavelength into the NIR region, a β-gal-active probe QM-HBT-βgal was elaborately synthesized by introducing the 2-(2-hydroxyphenyl) benzothiazole group as an external π-conjugated structure (Fig. 5b).[64] The results of the Cell experiment revealed that QM-HBT-βgal could realize long-term NIR fluorescence imaging in SKOV-3 cells. Considering the high performance of QM-HBT-βgal and QM-βgal, it was believed that the AIE-active strategy provides a new pathway to design enzyme-activatable probes for on-site sensing and long-term tracking in living samples.

5. Activatable probes from NIR-I to NIR-II imaging

The above mentioned activatable probes with NIR-I emission (650–900 nm) show potential *in vivo* applications for living cells and organisms, while NIR-II imaging could provide greater tissue penetration with markedly suppressed photon scattering and significant improvements in spatial resolution with zero-autofluorescence in mammals. Intriguingly, fluorescence imaging in the NIR-II spectrum (1000–1700 nm) opens a new pathway for deep-tissue biological exploration.[65,66] Nowadays, the primary challenge for NIR-II imaging is the limited availability of high-performance NIR-II fluorophores with both high brightness and biocompatibility. And various inorganic materials, such as quantum dots and lanthanide-doped nanoparticles, have also been explored as high spatial NIR-II contrasts. It should be noted that their long-term health risks due to the non-biodegradable feature need to be carefully considered.[67–69] To date, the design of small molecule-based organic fluorophores for NIR-II imaging, especially to *in vivo* monitor β-gal activities is still a huge challenge.

Towards enzyme-activated NIR-II probes, Zhao *et al.* established a universal platform with tunable emission from the NIR-I to the NIR-II region.[70] The emission of BODIPY-based fluorophores (EW-BOD-SH) was effectively red-shifted to a longer wavelength *via* incorporating an electron-withdrawing group into the 3-position of the BODIPY core, which exhibited a long tail falling into the NIR-II region (1000–1300 nm) (Fig. 7a). Furthermore, this platform was engineered by attaching enzymic substrates into EW-BOD-SH through a self-immolative benzyl thioether linking spacer (Fig. 7b). When the designed probes were catalyzed and triggered by the specific enzyme, they would subsequently undergo a 1,6-elimination reaction to liberate the sulfur atom of thiol-modified BODIPY with enhanced electron-donating ability, thereby ultimately generating desired NIR emission with large Stokes shifts. In this way,

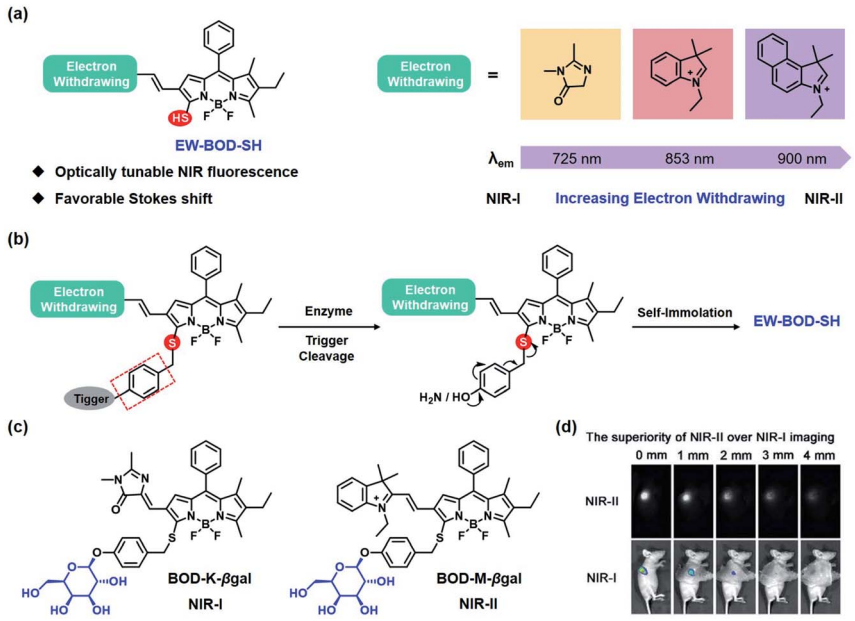

Fig. 7 The strategy of activatable probes from NIR-I to NIR-II imaging: (a) rational molecular design of fluorescent probes (EW-BOD-SH) from NIR-I to NIR-II by introducing an enhanced electron-withdrawing group. (b) Self-immolative pathway of enzyme-activated probes. (c) The chemical structure of the NIR-I probe (BOD-K-βgal) and NIR-II probe (BOD-M-βgal). (d) NIR-I and NIR-II imaging of living mice.

diverse activatable probes could be designed for the NIR-I/NIR-II fluorescence sensing of enzymes (such as NTR, NQO1 and ALP).

More importantly, using a similar design strategy, Gu and co-workers successfully developed two turn-on NIR-I and NIR-II probes (BOD-K-βgal and BOD-M-βgal) to recognize β-gal in ovarian cancers (Fig. 7b), which were also incorporated with a D-galactose residue as a β-gal activatable trigger.[71] Upon titration with β-gal, BOD-K-βgal and BOD-M-βgal displayed significant turn-on NIR-I or NIR-II responses, respectively. Furthermore, the *in vivo* ovarian tumor imaging was carried out in the SKOV3 subcutaneous xenograft nude mice. As shown in Fig. 7d, the obvious strong NIR-II signals of BOD-M-βgal could be observed even at a 2 mm depth, but the NIR-I signals of BOD-K-βgal were almost undetected even at 1 mm. These results further demonstrated that NIR-II imaging could penetrate deeper tissue and provide higher resolution than NIR-I imaging because of almost zero-autofluorescence and markedly suppressed photon scattering.

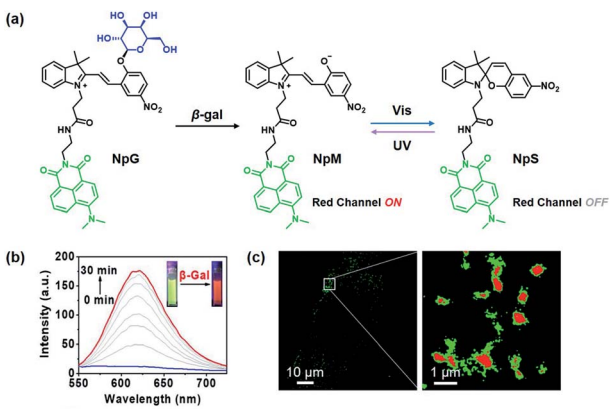

Fig. 8 (a) Fluorescence mechanism of photochromic probe NpM@HSA. Fluorescence response (b) and super-resolution imaging (c) of β-gal in senescent cells.

6. Dual-mode probes with AIE-active fluorescence and enriched chemiluminescence

Over the past decades, optical imaging (*e.g.* super-resolution imaging, photoacoustic (PA) imaging and chemiluminescence (CL) imaging) and other noninvasive imaging modalities (*e.g.* MRI and PET) have been rapidly developed for disease diagnosis and therapeutic intervention, thereby providing tremendous opportunities to monitor *in vivo* β-gal activity. For instance, He and Zhang *et al.* reported a photochromic fluorescent probe (NPG) for the super-resolution imaging of β-gal (Fig. 8).[72] Due to the excellent photoswitching properties of spiropyran-based dye (merocyanine ↔ spiropyran), NPG could overcome the diffraction limit of light and visualize the β-gal distribution with nanoscale precision. Very recently, Chan *et al.* introduced a new photoacoustic scaffold (PA-HD) by reasonable modification of hemicyanine dye (O-HD) (Fig. 9a):[73] replacing the oxygen atom with the sulfur atom to extend the absorption wavelength, enhance the extinction coefficient and attenuate the fluorescence quantum yield; adding the chloro group to adjust the phenolic pK_a value ensures that PA-HD exists in deprotonated form after PA-HD-Gal reacts with β-gal in a physiological environment (Fig. 9b and c). Furthermore, PA-HD-Gal was successfully applied in PA imaging of β-gal detection (Fig. 9d).

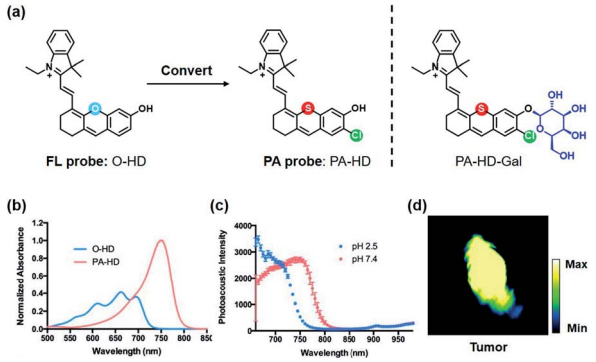

Fig. 9 (a) PA scaffold (PA-HD) by reasonable modification of hemicyanine dye (O-HD), and the PA probe (PA-HD-Gal) for β-gal. Absorption (b) and PA spectra (c) of PA-HD. (d) PA image of an *ex vivo* tumor.

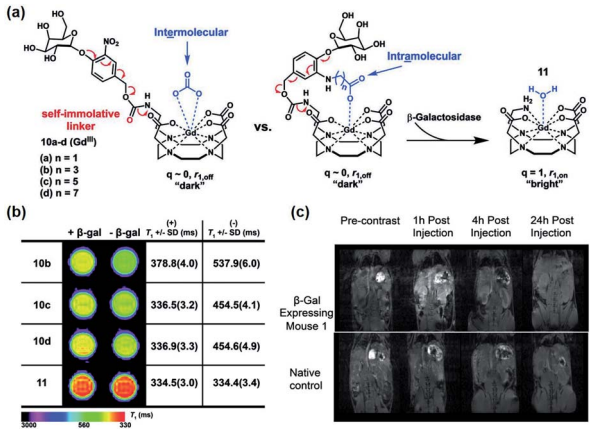

Fig. 10 (a) Self-immolative MRI contrast agents with intermolecular or intramolecular architecture for β-gal detection. (b) MR information of (10b–d) ±β-gal at 7 T. (c) MR images of living mice.

Given the advantage of the tissue-penetration depth of magnetic resonance imaging (MRI), Meade *et al.* developed a series of self-immolative β-gal-responsive contrast agents, and synthesized intermolecular and intramolecular architectures to optimize the coordination of water to Gd^{3+} (Fig. 10a and b).[13] Among them, 6-C pendant carboxylate (10c) was demonstrated as an effective MR contrast agent in the mouse model, which exhibits a visible MR signal at the 4 h time point (Fig. 10c). Consequently, considering the diversity of imaging modalities, it would be a powerful strategy to design β-gal-activatable probes with synergetic fluorescence and other imaging modalities.

Recently, some researchers focus on CL imaging which produces photons through specific chemical reactions rather than light excitation. Because CL imaging doesn't require an exogenous excitation light, the limitations from tissue autofluorescence and light scattering could be effectively avoided, thus obtaining a much higher signal-to-noise ratio.[74–76] However, current conventional CL probes, such as oxalate esters and luminol, were activated by the oxidation reaction and limited to the detection of oxidative species, making them difficult to real-time sense chemical or biological species. Schaap's adamantylidene-1,2-dioxetane with an analyte-responsive phenol trigger moiety emerged as a favored platform for CL imaging (Fig. 11a).[77–79] Upon the removal of the trigger moiety, the resulting phenolate intermediate is unstable and undergoes an electron transfer event and decomposition, accompanied by the blue glow-type emission.

Based on Schaap's dioxetane, many dioxetane probes were developed for a variety of analytes, including β-gal discussed here. For example, Mason and co-workers used the commercially chemiluminescent probe (Galacton) together with the addition of a surfactant-dye adduct for *in vivo* detection of β-gal. Moreover, in order to extend light emission to the NIR region, Shabat and co-workers designed the probe DCM-gal-C through

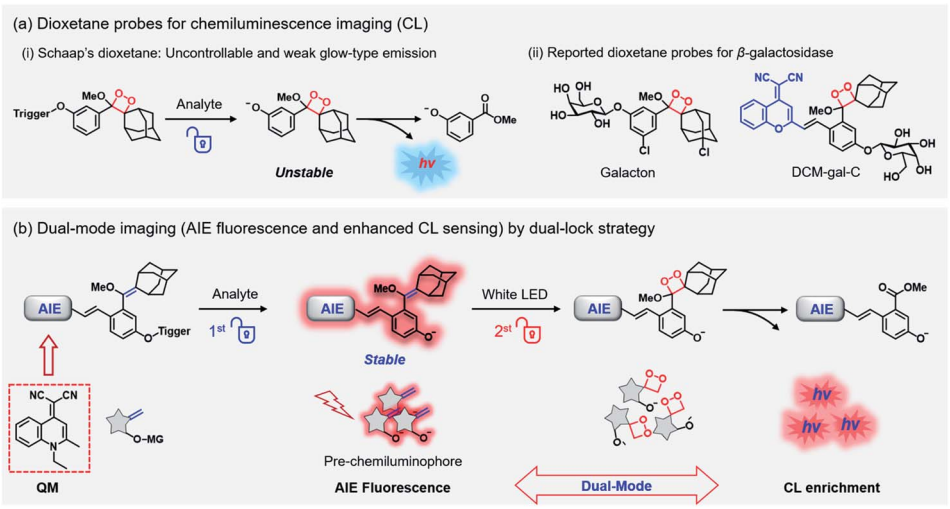

Fig. 11 Dual-mode probes with AIE-active fluorescence and enriched chemiluminescence sensing: (a) previous dioxetane probes for CL imaging: (i) Schaap's dioxetane and (ii) previous dioxetane probes for β-gal. (b) Dual-lock design strategy of dual-modal probes with AIE fluorescence and enriched chemiluminescence imaging.

integrating the DCM unit as an extended π-electron system at the para position of Schaap's 1,2-dioxetanes.

Although CL imaging could provide ultra-sensitive detection signals, it's still difficult to achieve longitudinal study in a dynamic biological environment due to its single-time output pattern. Considering that fluorescence imaging could obtain real-time feedback through light repeated excitation, the combination of CL imaging and fluorescence imaging into one unimolecular system could simultaneously meet the requirement of ultra-sensitive and real-time detection. Besides, these dioxetane-based probes produced only a sustained but weak CL signal because of their uncontrollable photon release, which immensely limits their practical application.

Towards this end, Guo *et al.* presented a dual-lock strategy to construct dual-mode probes with sequential trigger activation, exhibiting AIE-active fluorescence and enriched CL signals (Fig. 11b).[80] Specifically, the recognition moiety as the first lock was triggered by the analytes, leading to the generation and accumulation of stable pre-chemiluminophores. Owning to the double bond replacing the high-energy dioxetane group and the accumulation of AIEgens QM, pre-chemiluminophores could display better stability than reported dioxetane probes, and then generated stronger emission under light excitation. Subsequently, the electron-rich double bond as the second lock was triggered by irradiation with white LED light, thereby forming 1,2-dioxetane accompanied by bright and enriched CL signals. Based on this dual-mode imaging of dual-lock sequential control, they realized accurate *in vivo* sensing of β-gal. It was believed that this dual-lock strategy could expand the analytical toolboxes in biological research and clinical trials.

7. Summary and outlook

In this review, we summarized the latest studies on β-gal-activatable probes: from turn-on mode to ratiometric mode for reliable quantitative detection; AIE-active probes for on-site sensing and long-term tracking; from NIR-I imaging to NIR-II imaging for deeper tissue penetration and higher spatial resolution; dual-mode chemo-fluoro-luminescence signals for ultra-sensitive and real-time detection. Among them, our emphasis was on the rational design strategy for NIR fluorescence imaging, because NIR photons can relatively penetrate deep tissue and decrease background interference.

Although remarkable progress has been made for tracking β-gal, there are still many opportunities and challenges: (i) designing high-performance small-molecular NIR-II platforms with better fluorescence quantum yields and longer wavelength. The current reported NIR-II organic fluorophores always need a complicated synthetic procedure but just possess low quantum yield and little coverage in the NIR-II window, which still limits their application *in vivo*. It is imperative to develop a new strategy of simple structural design and easy modification of NIR-II dyes with brightness and longer emission. (ii) Integrating multiple imaging modalities (*e.g.* MRI, PET, CT, photoacoustic and fluorescence imaging) into a unimolecular system for the synergetic detection of β-gal. (iii) Distinguishing human endogenous β-gal from β-gal of other species. For the study of human β-gal, bacterial β-gal, especially *E. coli* β-gal, is habitually used as the substitute enzyme, but there is still structural difference between them. It is worth developing high-performance probes for the detection of human β-gal activity. We anticipate that these rational strategies for the probes would bring more breakthroughs in β-gal detection and related biological applications in the future.

Author contributions

Y. Yao wrote the manuscript. Z. Guo supervised this project. All the authors discussed and polished the manuscript.

Conflicts of interest

The authors declare no competing financial interest.

Acknowledgements

This work was supported by the National Natural Science Foundation of China (21878087, 21908060), the Innovation Program of Shanghai Municipal Education Commission (2019-01-07-00-02-E00060), Shuguang Program (18SG27), the Fundamental Research Funds for the Central Universities.

Notes and references

1 S. K. Chatterjee, M. Bhattacharya and J. J. Barlow, *Cancer Res.*, 1979, **39**, 1943–1951.
2 G. P. Dimri, X. Lee, G. Basile, M. Acosta, G. Scott, C. Roskelley, E. E. Medrano, M. LINskENs, I. Rubelj and O. Pereira-Smith, *Proc. Natl. Acad. Sci. U. S. A.*, 1995, **92**, 9363–9367.
3 B. Y. Lee, J. A. Han, J. S. Im, A. Morrone, K. Johung, E. C. Goodwin, W. J. Kleijer, D. DiMaio and E. S. Hwang, *Aging Cell*, 2006, **5**, 187–195.
4 D. Asanuma, M. Sakabe, M. Kamiya, K. Yamamoto, J. Hiratake, M. Ogawa, N. Kosaka, P. L. Choyke, T. Nagano and H. Kobayashi, *Nat. Commun.*, 2015, **6**, 1–7.
5 C.-H. Tung, Q. Zeng, K. Shah, D.-E. Kim, D. Schellingerhout and R. Weissleder, *Cancer Res.*, 2004, **64**, 1579–1583.
6 T. S. Wehrman, G. von Degenfeld, P. O. Krutzik, G. P. Nolan and H. M. Blau, *Nat. Methods*, 2006, **3**, 295–301.
7 M. Kamiya, H. Kobayashi, Y. Hama, Y. Koyama, M. Bernardo, T. Nagano, P. L. Choyke and Y. Urano, *J. Am. Chem. Soc.*, 2007, **129**, 3918–3929.
8 K. Owada-Makabe, Y. Tsubota, K. Yukawa, N. Kakimoto, X.-M. Liang, M. Ichinose and M. Maeda, *Neurosci. Lett.*, 2005, **378**, 18–21.
9 J. Wang, L. Wu, J. Ren and X. Qu, *Small*, 2012, **8**, 259–264.
10 B. V. Chikkaveeraiah, A. A. Bhirde, N. Y. Morgan, H. S. Eden and X. Chen, *ACS Nano*, 2012, **6**, 6546–6561.
11 Y. Zhou, H. Yin, X. Li, Z. Li, S. Ai and H. Lin, *Biosens. Bioelectron.*, 2016, **86**, 508–515.
12 S. Celen, C. Deroose, T. d. Groot, S. K. Chitneni, R. Gijsbers, Z. Debyser, L. Mortelmans, A. Verbruggen and G. Bormans, *Bioconjugate Chem.*, 2008, **19**, 441–449.

13 L. M. Lilley, S. Kamper, M. Caldwell, Z. K. Chia, D. Ballweg, L. Vistain, J. Krimmel, T. A. Mills, K. MacRenaris, P. Lee, E. A. Waters and T. J. Meade, *Angew. Chem., Int. Ed.*, 2020, **59**, 388–394.
14 A. Y. Louie, M. M. Hüber, E. T. Ahrens, U. Rothbächer, R. Moats, R. E. Jacobs, S. E. Fraser and T. J. Meade, *Nat. Biotechnol.*, 2000, **18**, 321–325.
15 J.-X. Yu, V. D. Kodibagkar, R. R. Hallac, L. Liu and R. P. Mason, *Bioconjugate Chem.*, 2012, **23**, 596–603.
16 H. W. Lee, C. H. Heo, D. Sen, H.-O. Byun, I. H. Kwak, G. Yoon and H. M. Kim, *Anal. Chem.*, 2014, **86**, 10001–10005.
17 W.-H. Zhu, M. Li and T. Gao, *Sci. Sin.: Chim.*, 2017, **47**, 898–905.
18 W. Sun, S. Guo, C. Hu, J. Fan and X. Peng, *Chem. Rev.*, 2016, **116**, 7768–7817.
19 D. Wu, A. C. Sedgwick, T. Gunnlaugsson, E. U. Akkaya, J. Yoon and T. D. James, *Chem. Soc. Rev.*, 2017, **46**, 7105–7123.
20 Z. Guo, S. Park, J. Yoon and I. Shin, *Chem. Soc. Rev.*, 2014, **43**, 16–29.
21 Z. Zhou, J. Song, L. Nie and X. Chen, *Chem. Soc. Rev.*, 2016, **45**, 6597–6626.
22 A. K. East, M. Y. Lucero and J. Chan, *Chem. Sci.*, 2021, **12**, 3393–3405.
23 P. Zhang, Z. Guo, C.-X. Yan and W.-H. Zhu, *Chin. Chem. Lett.*, 2017, **28**, 1952–1956.
24 C. Yan, L. Shi, Z. Guo and W.-H. Zhu, *Chin. Chem. Lett.*, 2019, **30**, 1849–1855.
25 Y. V. Suseela, N. Narayanaswamy, S. Pratihar and T. Govindaraju, *Chem. Soc. Rev.*, 2018, **47**, 1098–1131.
26 Y. Zhou, P. Li, X. Wang, C. Wu, N. Fan, X. Liu, L. Wu, W. Zhang, W. Zhang, Z. Liu and B. Tang, *Chem. Sci.*, 2020, **11**, 12149–12156.
27 H. Xiao, P. Li, W. Zhang and B. Tang, *Chem. Sci.*, 2016, **7**, 1588–1593.
28 C. Chen, R. Tian, Y. Zeng, C. Chu and G. Liu, *Bioconjugate Chem.*, 2020, **31**, 276–292.
29 Y. Li, Y. Wu, J. Chen, J. Wan, C. Xiao, J. Guan, X. Song, S. Li, M. Zhang, H. Cui, T. Li, X. Yang, Z. Li and X. Yang, *Nano Lett.*, 2019, **19**, 5806–5817.
30 X. Deng, Z. Yin, J. Lu, X. Li, L. Shao, C. Zhao, Y. Yang, Q. Hu, Y. Wu and W. Sheng, *Adv. Sci.*, 2018, **5**, 1700542.
31 J. Zhou and H. Ma, *Chem. Sci.*, 2016, **7**, 6309–6315.
32 M. Kamiya, D. Asanuma, E. Kuranaga, A. Takeishi, M. Sakabe, M. Miura, T. Nagano and Y. Urano, *J. Am. Chem. Soc.*, 2011, **133**, 12960–12963.
33 T. Egawa, Y. Koide, K. Hanaoka, T. Komatsu, T. Terai and T. Nagano, *Chem. Commun.*, 2011, **47**, 4162–4164.
34 O. Redy-Keisar, E. Kisin-Finfer, S. Ferber, R. Satchi-Fainaro and D. Shabat, *Nat. Protoc.*, 2014, **9**, 27–36.
35 D. Oushiki, H. Kojima, Y. Takahashi, T. Komatsu, T. Terai, K. Hanaoka, M. Nishikawa, Y. Takakura and T. Nagano, *Anal. Chem.*, 2012, **84**, 4404–4410.
36 J. Zhang, C. Li, C. Dutta, M. Fang, S. Zhang, A. Tiwari, T. Werner, F.-T. Luo and H. Liu, *Anal. Chim. Acta*, 2017, **968**, 97–104.
37 B. Lozano-Torres, I. Galiana, M. Rovira, E. Garrido, S. Chaib, A. Bernardos, D. Munoz-Espin, M. Serrano, R. Martinez-Manez and F. Sancenon, *J. Am. Chem. Soc.*, 2017, **139**, 8808–8811.
38 X. Li, Y. Pan, H. Chen, Y. Duan, S. Zhou, W. Wu, S. Wang and B. Liu, *Anal. Chem.*, 2020, **92**, 5772–5779.
39 X. Pang, Y. Li, Z. Zhou, Q. Lu, R. Xie, C. Wu, Y. Zhang and H. Li, *Talanta*, 2020, **217**, 121098.
40 Y. Guo, Y. Gao, Y. Hu, Q. Liu, X. Li, X. Li, C. Y. Kim, T. D. James, J. Li and X. Chen, *Angew. Chem., Int. Ed.*, 2021, **60**(19), 10756–10765.
41 M. H. Lee, J. S. Kim and J. L. Sessler, *Chem. Soc. Rev.*, 2015, **44**, 4185–4191.
42 X.-X. Zhang, H. Wu, P. Li, Z.-J. Qu, M.-Q. Tan and K.-L. Han, *Chem. Commun.*, 2016, **52**, 8283–8286.
43 E. J. Kim, R. Kumar, A. Sharma, B. Yoon, H. M. Kim, H. Lee, K. S. Hong and J. S. Kim, *Biomaterials*, 2017, **122**, 83–90.
44 Y. Li, H. Wang, J. Li, J. Zheng, X. Xu and R. Yang, *Anal. Chem.*, 2011, **83**, 1268–1274.
45 T. Komatsu, K. Kikuchi, H. Takakusa, K. Hanaoka, T. Ueno, M. Kamiya, Y. Urano and T. Nagano, *J. Am. Chem. Soc.*, 2006, **128**, 15946–15947.
46 X. Li, W. Qiu, J. Li, X. Chen, Y. Hu, Y. Gao, D. Shi, X. Li, H. Lin, Z. Hu, G. Dong, C. Sheng, B. Jiang, C. Xia, C.-Y. Kim, Y. Guo and J. Li, *Chem. Sci.*, 2020, **11**, 7292–7301.
47 L. Shi, C. Yan, Y. Ma, T. Wang, Z. Guo and W.-H. Zhu, *Chem. Commun.*, 2019, **55**, 12308–12311.
48 K. Gu, Y. Xu, H. Li, Z. Guo, S. Zhu, S. Zhu, P. Shi, T. D. James, H. Tian and W.-H. Zhu, *J. Am. Chem. Soc.*, 2016, **138**, 5334–5340.
49 C. W. Tang, S. A. VanSlyke and C. H. Chen, *J. Appl. Phys.*, 1989, **65**, 3610–3616.
50 *In vivo* Tracking β-galactosidase activity, *Nat. Methods*, 2016, **13**, 470, DOI: 10.1038/nmeth.3876.
51 Z. Thiel and P. Rivera-Fuentes, *Angew. Chem., Int. Ed.*, 2019, **58**, 11474–11478.
52 C. Yik-Sham Chung, G. A. Timblin, K. Saijo and C. J. Chang, *J. Am. Chem. Soc.*, 2018, **140**, 6109–6121.
53 Z. Gao, A. J. Thompson, J. C. Paulson and S. G. Withers, *Angew. Chem., Int. Ed.*, 2018, **130**, 13726–13729.
54 E. A. Halabi, Z. Thiel, N. Trapp, D. Pinotsi and P. Rivera-Fuentes, *J. Am. Chem. Soc.*, 2017, **139**, 13200–13207.
55 R. Yan, Y. Hu, F. Liu, S. Wei, D. Fang, A. J. Shuhendler, H. Liu, H. Y. Chen and D. Ye, *J. Am. Chem. Soc.*, 2019, **141**, 10331–10341.
56 J. Luo, Z. Xie, J. W. Y. Lam, L. Cheng, B. Z. Tang, H. Chen, C. Qiu, H. S. Kwok, X. Zhan, Y. Liu and D. Zhu, *Chem. Commun.*, 2001, **18**, 1740–1741.
57 Z. Zhao, H. Zhang, J. W. Y. Lam and B. Z. Tang, *Angew. Chem., Int. Ed.*, 2020, **59**, 9888–9907.
58 J. Mei, N. L. Leung, R. T. Kwok, J. W. Lam and B. Z. Tang, *Chem. Rev.*, 2015, **115**, 11718–11940.
59 Q. Xu, K.-A. Lee, S. Lee, K. M. Lee, W.-J. Lee and J. Yoon, *J. Am. Chem. Soc.*, 2013, **135**, 9944–9949.
60 L. Wang, L. Yuan, X. Zeng, J. Peng, Y. Ni, J. C. Er, W. Xu, B. K. Agrawalla, D. Su and B. Kim, *Angew. Chem., Int. Ed.*, 2016, **128**, 1805–1808.

61 G. Jiang, G. Zeng, W. Zhu, Y. Li, X. Dong, G. Zhang, X. Fan, J. Wang, Y. Wu and B. Z. Tang, *Chem. Commun.*, 2017, **53**, 4505–4508.
62 Z. Gao, H. Gao, D. Zheng, T. Xu, Y. Chen, C. Liang, L. Wang, D. Ding and Z. Yang, *Sci. China: Chem.*, 2020, **63**, 398–403.
63 K. Gu, W. Qiu, Z. Guo, C. Yan, S. Zhu, D. Yao, P. Shi, H. Tian and W.-H. Zhu, *Chem. Sci.*, 2019, **10**, 398–405.
64 W. Fu, C. Yan, Y. Zhang, Y. Ma, Z. Guo and W.-H. Zhu, *Front. Chem.*, 2019, **7**, 291.
65 F. Ding, Y. Zhan, X. Lu and Y. Sun, *Chem. Sci.*, 2018, **9**, 4370–4380.
66 S. Wang, B. Li and F. Zhang, *ACS Cent. Sci.*, 2020, **6**, 1302–1316.
67 G. Hong, A. L. Antaris and H. Dai, *Nat. Biomed. Eng.*, 2017, **1**, 1–22.
68 E. D. Cosco, A. L. Spearman, S. Ramakrishnan, J. G. P. Lingg, M. Saccomano, M. Pengshung, B. A. Arus, K. C. Y. Wong, S. Glasl, V. Ntziachristos, M. Warmer, R. R. McLaughlin, O. T. Bruns and E. M. Sletten, *Nat. Chem.*, 2020, **12**, 1123–1130.
69 E. D. Cosco, B. A. Arus, A. L. Spearman, T. L. Atallah, I. Lim, O. S. Leland, J. R. Caram, T. S. Bischof, O. T. Bruns and E. M. Sletten, *J. Am. Chem. Soc.*, 2021, **143**, 6836–6846.
70 R. Wang, J. Chen, J. Gao, J.-A. Chen, G. Xu, T. Zhu, X. Gu, Z. Guo, W.-H. Zhu and C. Zhao, *Chem. Sci.*, 2019, **10**, 7222–7227.
71 J. A. Chen, H. Pan, Z. Wang, J. Gao, J. Tan, Z. Ouyang, W. Guo and X. Gu, *Chem. Commun.*, 2020, **56**, 2731–2734.
72 X. Chai, H. H. Han, A. C. Sedgwick, N. Li, Y. Zang, T. D. James, J. Zhang, X. L. Hu, Y. Yu, Y. Li, Y. Wang, J. Li, X. P. He and H. Tian, *J. Am. Chem. Soc.*, 2020, **142**, 18005–18013.
73 S. H. Gardner, C. J. Brady, C. Keeton, A. K. Yadav, S. C. Mallojjala, M. Y. Lucero, S. Su, Z. Yu, J. S. Hirschi, L. M. Mirica and J. Chan, *Angew. Chem., Int. Ed.*, 2021, DOI: 10.1002/anie.202105905.
74 J. Huang and K. Pu, *Angew. Chem., Int. Ed.*, 2020, **59**, 11717–11731.
75 S. Gnaim, O. Green and D. Shabat, *Chem. Commun.*, 2018, **54**, 2073–2085.
76 N. Hananya and D. Shabat, *Angew. Chem., Int. Ed.*, 2017, **56**, 16454–16463.
77 A. P. Schaap, M. D. Sandison and R. S. Handley, *Tetrahedron Lett.*, 1987, **28**, 1159–1162.
78 A. P. Schaap, R. S. Handley and B. P. Giri, *Tetrahedron Lett.*, 1987, **28**, 935–938.
79 A. P. Schaap, T.-S. Chen, R. S. Handley, R. DeSilva and B. P. Giri, *Tetrahedron Lett.*, 1987, **28**, 1155–1158.
80 Y. Zhang, C. Yan, C. Wang, Z. Guo, X. Liu and W.-H. Zhu, *Angew. Chem., Int. Ed.*, 2020, **59**, 9059–9066.